Supporting information for

Selectivity Switch into Formation of Benzene by Surface Carbonates on Ceria in Catalytic Gas-Phase Oxidation of Benzyl Alcohol

Yihu Dai,[‡ac] Xin-Ping Wu, [‡b] Yu Tang,[a] Yanhui Yang,[c] Xue-Qing Gong,*[b] and Jie Fan*[a]

[a]Key Lab of Applied Chemistry of Zhejiang Province, Department of Chemistry, Zhejiang University, Hangzhou 310027, People's Republic of China

[b]Key Laboratory for Advanced Materials, Centre for Computational Chemistry and Research Institute of Industrial Catalysis, East China University of Science and Technology, Shanghai 200237, People's Republic of China

[c]School of Chemical and Biomedical Engineering, Nanyang Technological University, Singapore 637459, Singapore

[‡]Equal contribution for this work.

Experimental Details

Material Synthesis and Treatment

In a typical synthesis, 10 mmol of $Ce(NO_3)_3 \cdot 6H_2O$, 40 mmol of HOAc, 24 mmol of HCl, and 1.6 g of F127 ($EO_{96}PO_{70}EO_{96}$, MW = 12 000 g/mol) were dissolved in 30 mL of ethanol. The mixture was stirred vigorously for 2 h and transferred to a Petri dish (diameter 125 mm). The ethanol solution was evaporated at 40 - 60 °C with relative humidity of 30 - 80 %. After the solvent was evaporated, the mixture was transferred into a 65 °C oven and aged for 24 h. The as-synthesized mesostructured hybrids were calcined at 550 °C in air for 6 h (ramp rate 3 °C/min) to obtain the mesoporous CeO_2 catalyst.

In order to eliminate the adsorbed H_2O species and hydroxyl groups on the CeO_2 surface, the CeO_2 catalyst was outgassed by a mechanical pump at 723 °C for 0.5 h and then treated in O_2 at 600 °C for 24 h.[1] The outgassing process was repeated three times. The ex-situ IR spectrum and aerobic/anaerobic oxidation reaction of BA were proceeded after outgassing again at 723 °C for 30 min and cooling down in N_2 flow. The N_2 and O_2 gases were dried with molecular sieve and silica gel. Most of surface hydroxyl groups and adsorbed CO_2 molecules can be removed through this process, which is confirmed by FT-IR (Figure S21).

As reference sample, CO_2-treated meso-CeO_2 was prepared by calcination under 30 mL/min of CO_2 flow at 240 °C for 36 h and H_2-reduced meso-CeO_2 was obtained by calcination under 30 mL/min of H_2 flow at 550 °C for 6 h.

Catalytic Reaction

Benzyl alcohol (99.8 %, from Sigma-Aldrich) was used without further purification. Pure oxygen gas was used as the oxidant. The oxidation was performed using a conventional continuous-flow fixed-bed glass vertical reactor (h = 150 mm, i.d. = 10 mm), fitted with a glass frit holding 0.2 - 0.5 g of catalysts. The catalyst was preheated at 110 °C for 1 h with oxygen flow. The reaction was started by charging benzyl alcohol into the reactor. The charging rates of benzyl alcohol (0.3 - 1.8 mL/h) and oxygen gas (0.5 - 20.0 mL/min) were controlled by a syringe pump and mass flow instrument, respectively. Liquid vaporization occurred on the reactor wall prior to the catalytic bed. Typical reaction temperature range was 203 - 300 ºC. The liquid products and unreacted benzyl alcohol were collected by using a cold trap. The liquid products were periodically collected during the reaction and quantitatively analyzed by an Agilent gas chromatograph 6890 equipped with an HP-5 capillary column (30 m x 0.32 mm) and flame ionization detector (FID). The gas products were in-situ analyzed by a mass spectrometer (Hiden analytical QGA). Dodecane was the internal standard to calculate liquid product distributions. The analysis of benzene needs combining of GC-FID and in-situ MS because benzene is highly volatile. The carbon balance is greater than 95 % in all reactions.

For the anaerobic oxidation of BA, 20.0 mL/min of pure N_2 was used as carrier gas. 0.25 g of catalyst was pretreated in N_2 at given temperature (240 or 300 ºC) for 1 h to remove residual air or water vapor before the anaerobic oxidation started. 0.4 mL/h of BA was controlled by a syringe pump. The products analysis is same as above.

Device Characterization

The XRD patterns were analyzed by a Rigaku Ultimate IV with Cu K α radiation. The TEM and HR-TEM images of catalysts were recorded on a JEOL JEM 3010 at 300 kV. Nitrogen adsorption isotherms were measured on a Micromeritics ASAP 2020 adsorption analyzer at -196 °C, and samples were outgassed under vacuum at 200 °C before the adsorption analysis. The XPS measurements were performed in a VG Scientific ESCALAB Mark II spectrometer equipped with two ultrahigh vacuum (UHV) chambers. All binding energies were referenced to the C1s peak at 284.6 eV. The IR spectra were recorded on a Perkin-Elmer Spectrum One FTIR Spectrometer equipped with DTGS detector at room temperature with KBr pellets (4000 - 450 cm^{-1}, resolution of 4 cm^{-1}).

The Raman measurements were performed on a Labor Raman HR-800 with laser excitations at 514.5 nm. The total reaction feeding gas was fixed at 20 ml/min by mass-flow controller under shifted gas atmospheres and the programmed temperature rise was set in in-situ Raman experiments. The BA was introduced into in-situ cell by importing carry gas (O_2 or N_2) to generate babble in pure BA liquid. The four sequent stages were O_2 for 40 min, O_2+BA for 60 min, N_2+BA for 240 min and O_2+BA for 90 min, performed at 220, 240 and 260 ºC, respectively. The samples were swept with pure N_2 at 200 ºC to remove surface impurities before data record.

Computational Details for DFT Calculations

Spin-polarized density functional theory (DFT) calculations corrected by London dispersion of DFT-D scheme[2] and on-site Coulomb interaction (DFT+U) were performed with the Perdew-Burke-Ernzerhof (PBE) functional by using the Vienna ab initio Simulation Package (VASP).[3] According to the previous study,[4] dispersion coefficient (C_6) and vdW radii (R_0) for Ce were set to 20.00 J nm^6 mol^{-1} and 186.0 pm, respectively. Default values given by Grimme[1] were employed to C_6 and R_0 parameters of other elements. For the localized 4*f* electron, we used a Hubbard U of 5.0 eV.[5] Valence-core interaction was described by the project-augmented wave (PAW) method[6] at a kinetic energy cutoff of 400 eV with Ce (5s, 5p, 6s, 5d, 4f), O (2s, 2p), C (2s, 2p), and H (1s) shells being treated as valence electrons. The calculated lattice parameter is 5.440 Å, which is in good agreement with the experimental value of 5.411 Å.[7]

A 9 atomic layer slab with surface cell of 4×4 was used for the CeO_2(111) surface. The bottom tri-layer was fixed in all calculations to estimate bulk parameters. A large vacuum gap (>10 Å) was used to avoid interactions between slabs.

For the Brillouin-zone integration, we used a 1×1×1 k-mesh. A larger k-mesh grid of 2×2×1 was also tested for the calculation of CO adsorption energies, and it has been found that 1×1×1 and 2×2×1 k-mesh grids give nearly identical results (Table S4), indicating that 1×1×1 k-mesh grid should be enough for the calculations in this work. Structure optimizations were performed until the forces on each ion were less than 0.02 eVÅ^{-1}.

Adsorption energies of adsorbates (E_{ads}) and oxygen vacancy formation energies (E_{ov}) were calculated as follows:

$$E_{ads} = E_{ad} + E_{sub} - E_{ad/sub},$$

$$E_{ov} = 0.5E_{O2} + E_{ov/sub} - E_{sub},$$

where E_{ad}, E_{sub}, $E_{ad/sub}$, E_{O2} and $E_{ov/sub}$ are the DFT total energies of the gas-phase adsorbate, the substrate, the adsorption complex, gas-phase O_2 and the reduced substrate, respectively.

Thermodynamic analyses were based on calculating the surface free energy change per unit area ($\Delta\gamma$):

$$\Delta\gamma(p,T) = \frac{1}{A}\Big\{G[CO_x/CeO_2](p,T) - G[CeO_2](p,T) - \mu[C](p,T) - \frac{n}{2}\mu[O_2](p,T)\Big\},$$

where A is the area of one side of the surface cell, $G[CO_x/CeO_2](p,T)$ and $G[CeO_2](p,T)$ are the Gibbs free energy of carbonate species depositedCeO$_2$(111) and clean CeO$_2$(111), respectively, $\mu[C](p,T)$ and $\mu[O_2](p,T)$ are the chemical potentials of the carbon atom and gas-phase O_2, respectively.

$\mu[O_2](p,T)$ can be calculated as following:

$$\frac{1}{2}\mu[O_2](p,T) = \frac{1}{2}E[O_2] + \Delta\mu[O](p,T) = \frac{1}{2}E[O_2] + \frac{1}{2}\Big\{H(p^0,T) - H(p^0,0K) - TS(p^0,T) + K_BTln\frac{p}{p^0}\Big\}.$$

In addition, Gibbs free energies of the solid components can be equal to the DFT total energies and $\mu[C](p,T)$ can be equal to the DFT total energy of the C atom ($E[C]$). Accordingly, we obtained the following equation:

$$\Delta\gamma(p,T) = \frac{1}{A}\Bigg\{E[CO_x/CeO_2] - E[CeO_2] - E[C] - \frac{n}{2}E[O_2]$$

$$-\frac{n}{2}\Big\{H(p^0,T) - H(p^0,0K) - TS(p^0,T) + K_B T ln\frac{p}{p^0}\Big\}\Bigg\}$$

Structure information of carbonate species on CeO_2(111)

Five stable structures A-E are discussed in this work. Structure B can be regarded as a bent CO_2 attached to CeO_2(111). Structures A and C have similar CO_3 groups with structure B, and the only difference among these three structures is the local structure near the CO_3 group as it is a surface O atom, O_2^{2-} or O vacancy beside. Structure D occurs in the way that a carbon atom sits on top of one sub-surface O of clean CeO_2(111). The carbon then binds with three neighboring top-surface O atoms to form the CO_3 group, which also brings drastic distortion to the surface bonds of these O. Structure E occurs as the result of formation of a sub-surface O vacancy at structure D. Charge analyses indicated that two, four and six Ce^{3+} are generated at structures C, D and E, respectively. Side views of structures A-E are in Figure S14. Ce^{3+} patterns of structures C, D and E are shown in Figure S15.

References

(1) C. Li, Y. Sakata, T. Arai, K. Domen, K. I. Maruya and T. Onishi, *J. Chem. Soc., Faraday Trans.*, **1989,** *85*, 929-943.

(2) S. Grimme *J. Comput. Chem.* **2006,** *27*, 1787-1799.

(3) (a) G. Kresse and J. Furthmüller, J. *Comput. Mater. Sci.* **1996,** *6*, 15-50; (b) G. Kresse and J. Hafner, *Phys. Rev. B* **1994,** *49*, 14251-14269.

(4) C. Penschke, J. Paier and J. Sauer, *J. Phys. Chem. C* **2013,** *117*, 5274-5285.

(5) (a) M. Nolan, S. C. Parker and G. W. Watson, *Surf. Sci.* **2005,** *595*, 223-232; (b) Nolan, M.; Grigoleit, S.; Sayle, D. C.; Parker, S. C.; Watson, G. W. *Surf. Sci.* **2005,** *576*, 217-229.

(6) P. E. Blöchl, *Phys. Rev. B* **1994,** *50*, 17953-17979.

(7) E. A. Kümmerle and G. Heger, *J. Solid. State Chem.* **1999,** *147*, 485-500.

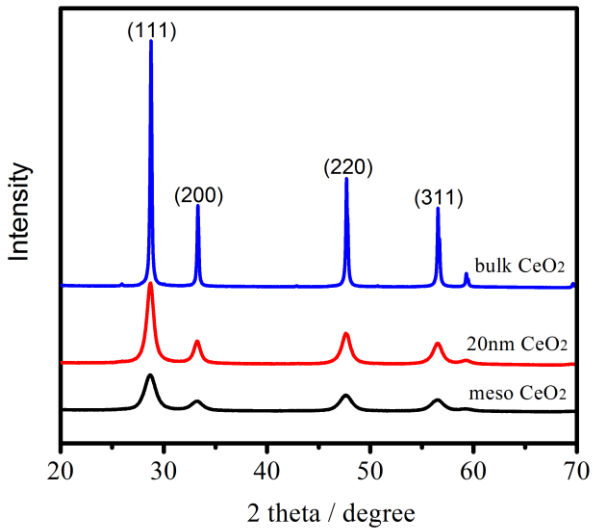

Figure S1. Wide-angle X-ray diffraction patterns of as-prepared mesoporous CeO_2, commercial 20 nm CeO_2 (from Sigma), and commercial bulk CeO_2 (from Sigma).

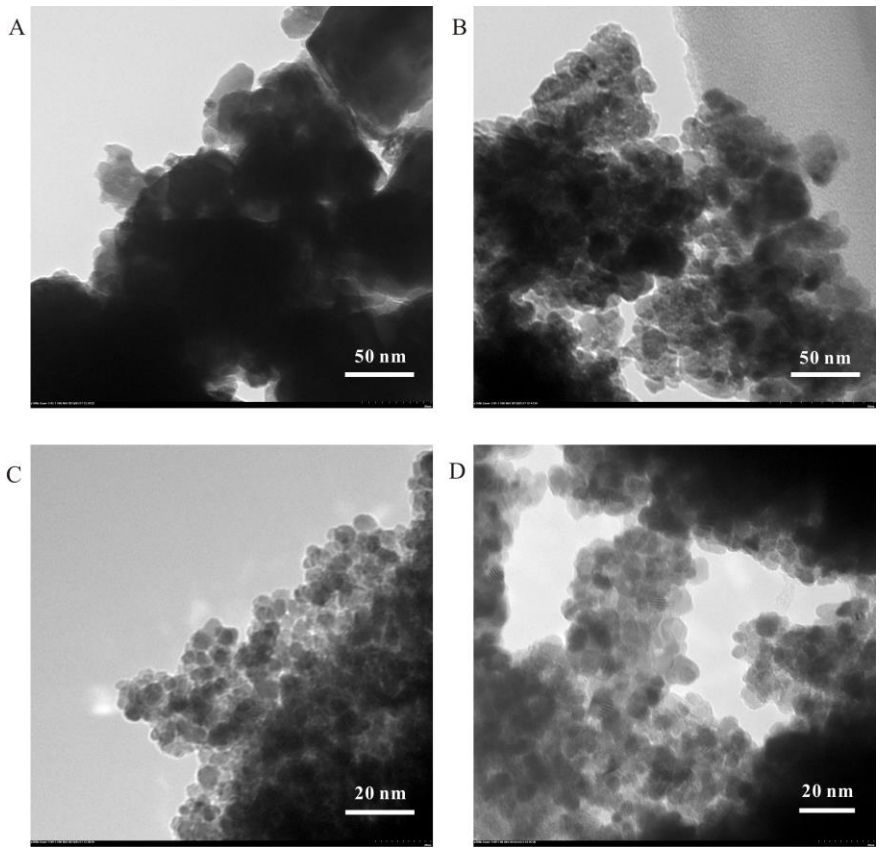

Figure S2. TEM images of (A) commercial bulk CeO_2, (B) commercial 20 nm CeO_2, and (C, D) as-prepared mesoporous CeO_2.

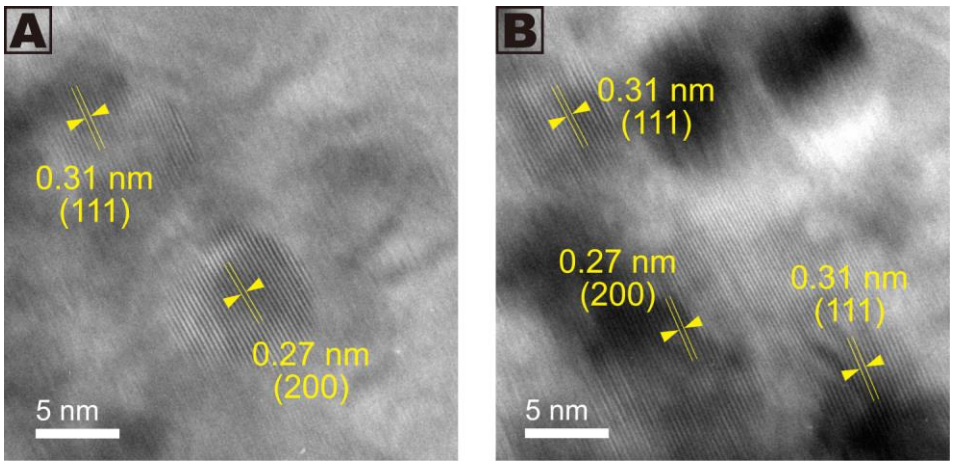

Figure S3. HR-TEM images of as-prepared mesoporous CeO_2 catalyst.

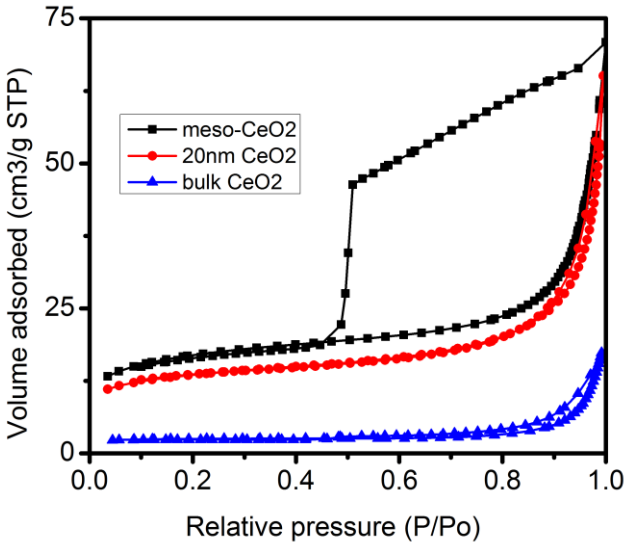

Figure S4. Nitrogen sorption isotherms of as-prepared mesoporous CeO_2, commercial 20 nm CeO_2, and commercial bulk CeO_2.

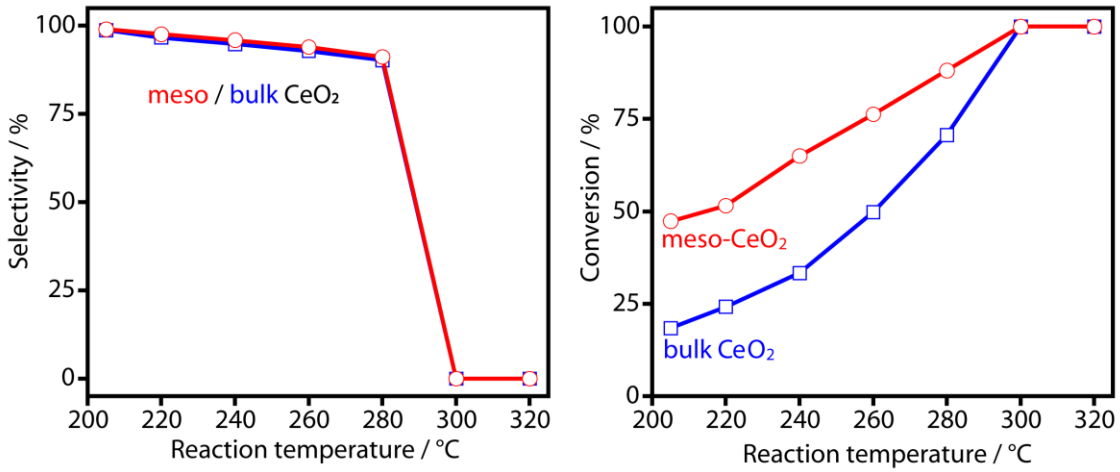

Figure S5. The selectivity toward BAD and conversion of BA as a function of the reaction temperature. Reaction conditions: catalyst = 0.3 g, BA = 0.3 mL/h, and O_2 = 20 mL/min.

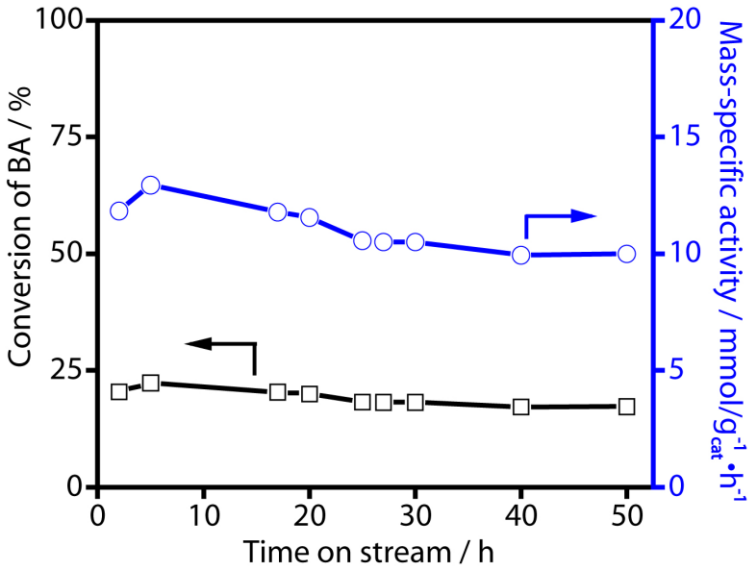

Figure S6. Reaction stability of meso-CeO_2 catalyst for a long-term reaction towards selective gas-phase oxidation of BA. Reaction conditions: catalyst = 0.2 g, BA = 1.0 mL/h, and O_2 = 20 mL/min, at 240 ºC.

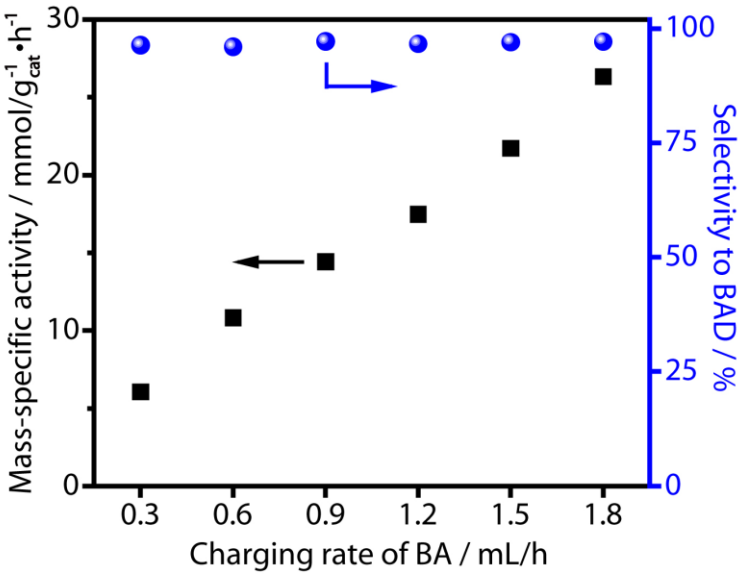

Figure S7. The selectivity toward BAD and mass-specific activity as a function of the charging rate of BA. Reaction conditions: catalyst, 0.3 g; BA, 0.3 - 1.8 mL/h; O_2, 20.0 mL/min; temperature, 240 °C.

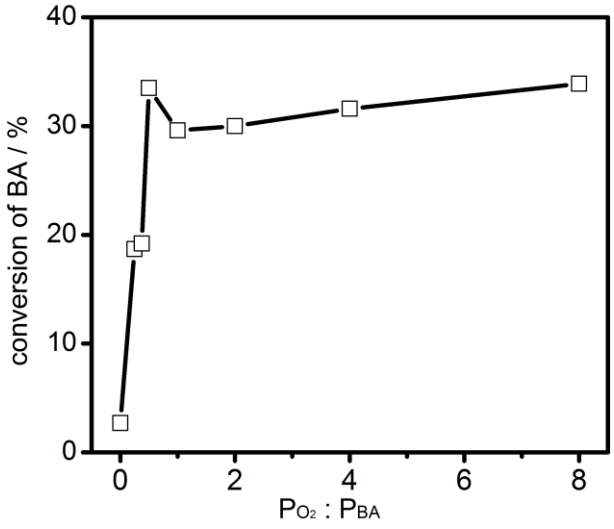

Figure S8. The conversion of BA as a function of partial pressure of O_2 for BA oxidation reaction. Reaction temperature is 240 °C.

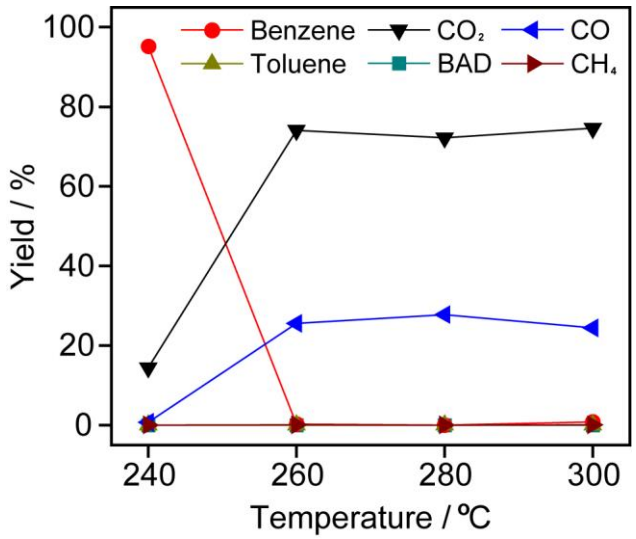

Figure S9. The yields of products in BA aerobic oxidation over CO_3-CeO_2 (meso-CeO_2 catalyst after 36 h of anaerobic oxidation of BA at 240 ºC) as a function of the reaction temperature. Reaction conditions: catalyst = 0.25 g, BA = 0.4 mL/h, and O_2 = 15.0 mL/min.

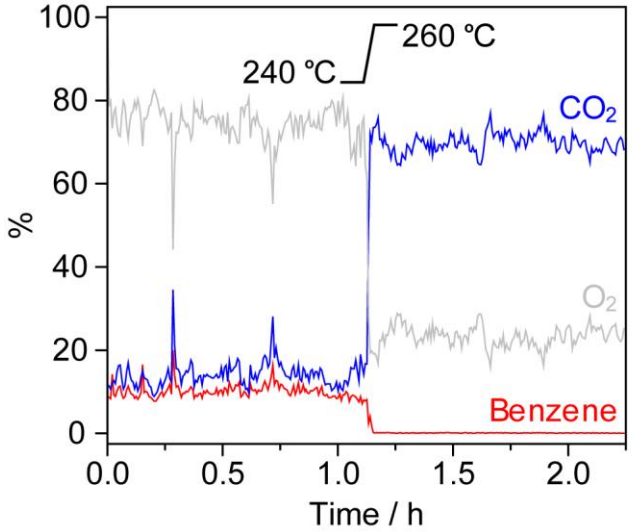

Figure S10. The generation of benzene/CO_2 at 240 ºC and the change of benzene-to-CO_2 at 260 ºC were obtained on meso-CeO_2 catalyst after 36 h of anaerobic oxidation of BA at 240 ºC. Reaction conditions: catalyst = 0.25 g, BA = 0.4 mL/h, and O_2 = 15.0 mL/min.

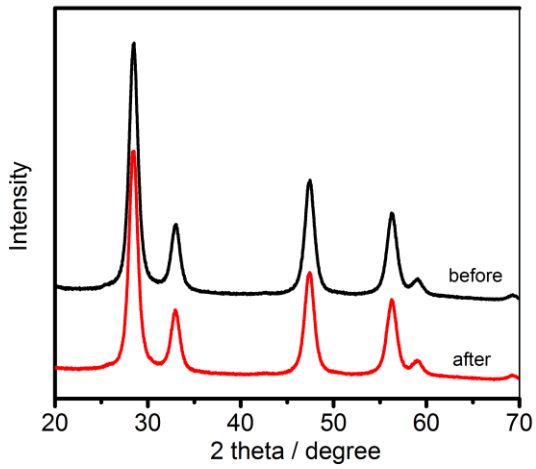

Figure S11. The XRD patterns of meso-CeO_2 catalyst before and after anaerobic (in pure N_2) gas-phase reaction of BA at 240 ^oC.

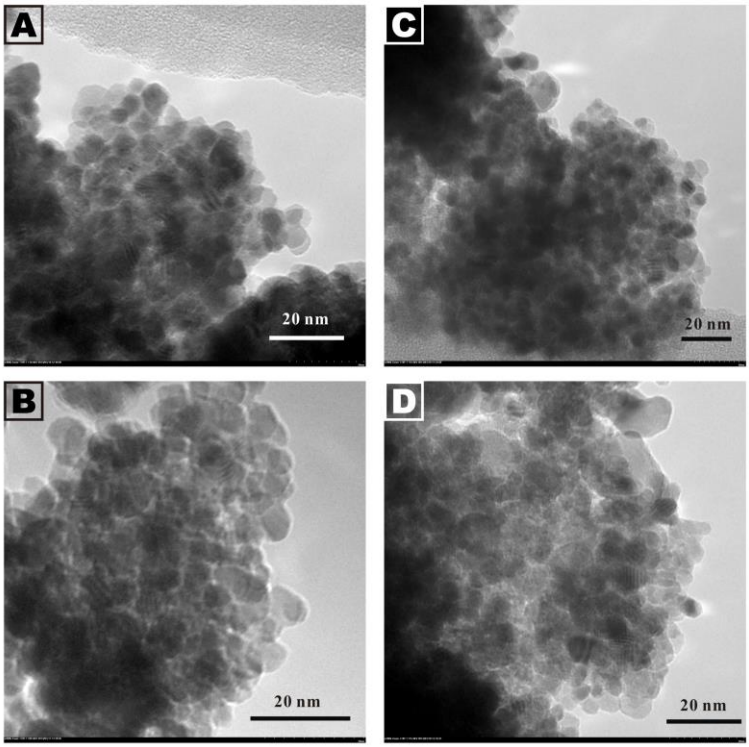

Figure S12. The TEM images of meso-CeO_2 catalyst (A-B) before and (C-D) after anaerobic (in pure N_2) gas-phase reaction of BA at 240 ^oC.

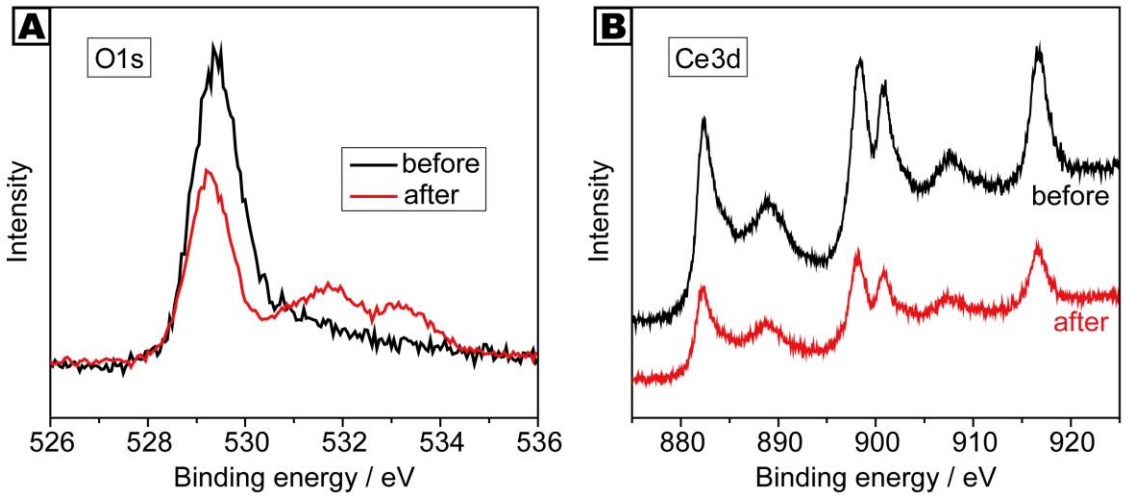

Figure S13. The XPS (A) O1s and (B) Ce3d spectra of meso-CeO_2 catalyst before and after gas-phase anaerobic (in N_2) reaction of BA at 240 ^oC.

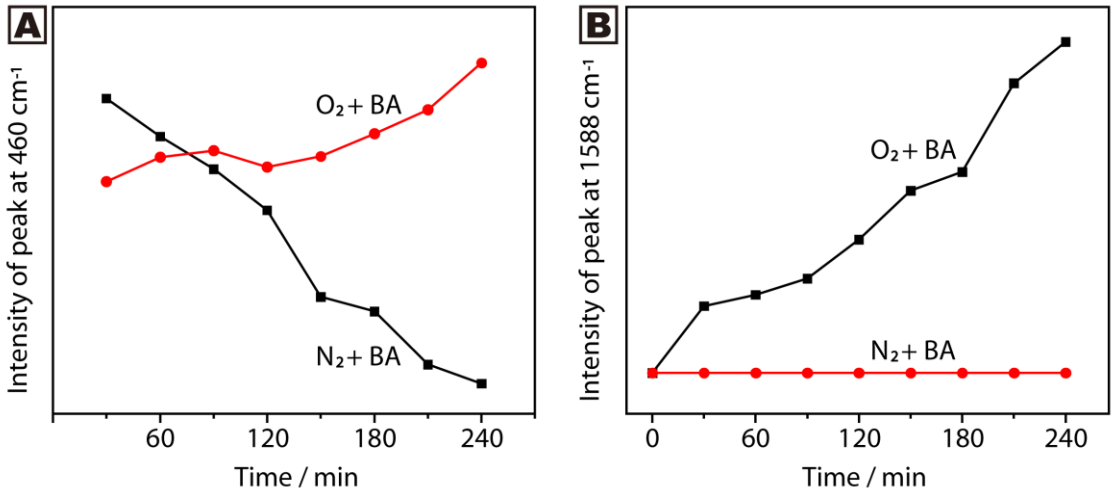

Figure S14. The intensity of Raman peak at 460 cm^{-1} (A) and 1588 cm^{-1} (B) as a function of reaction time under aerobic and anaerobic oxidation of BA at 240 ^oC for 240 min.

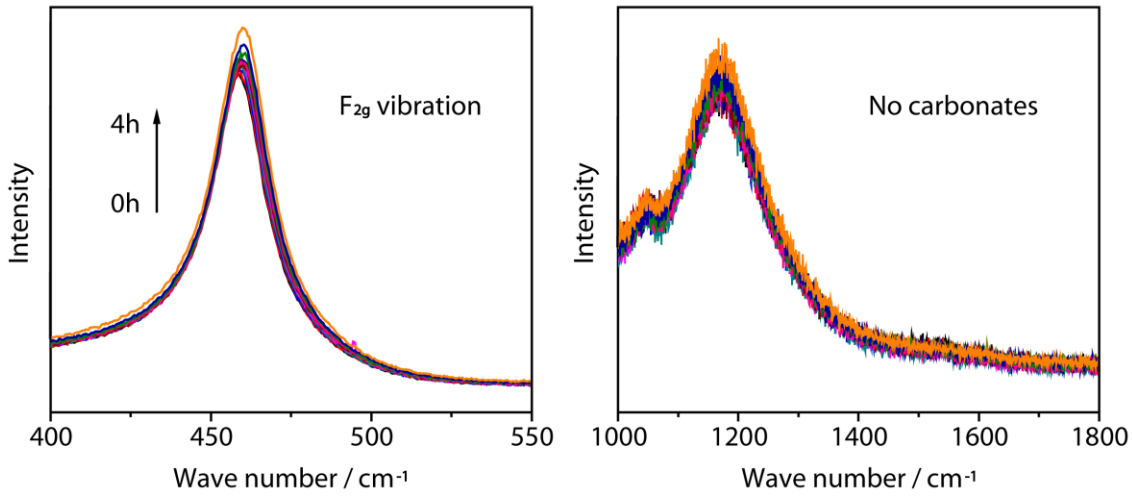

Figure S15. In-situ Raman spectra recorded during BA oxidation process over meso-CeO_2 catalyst in aerobic condition (O_2 + BA) at 240 ^oC for 240 min.

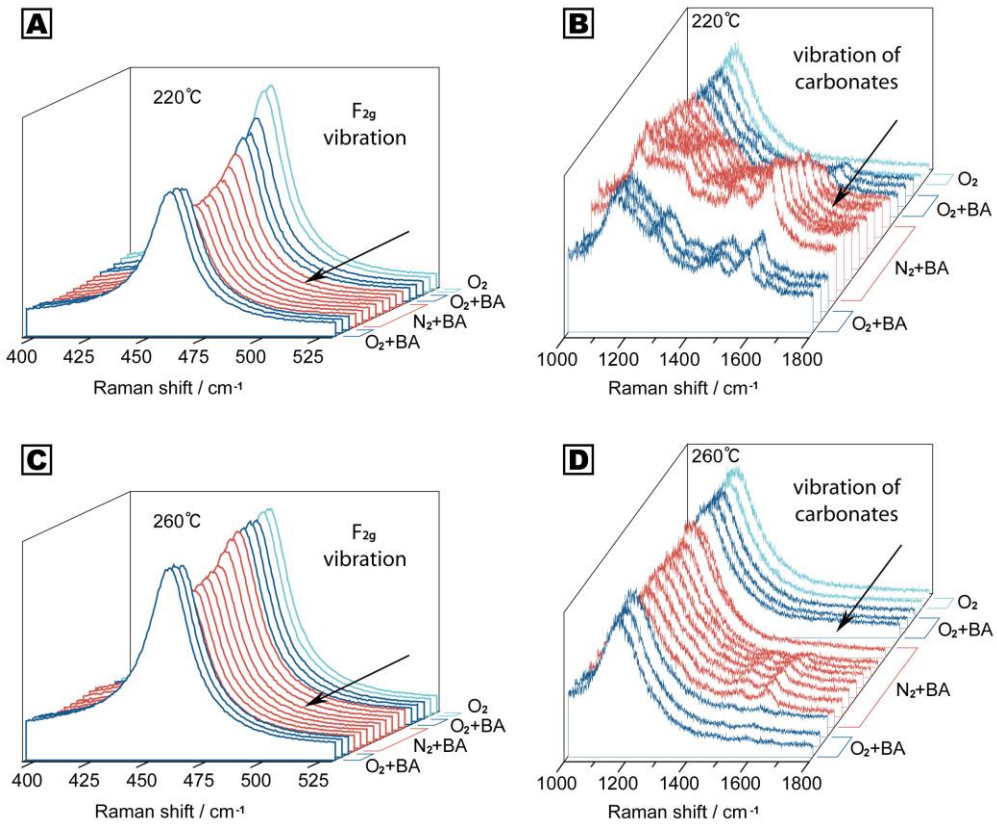

Figure S16. In-situ Raman spectra recorded during BA oxidation over meso-CeO_2 catalyst in four reaction conditions with gaseous atmospheres switched from pure O_2 (stage 1), O_2 + BA (stage 2), and N_2 + BA (stage 3) to O_2 + BA (stage 4). A and C present F_{2g} vibration situation of CeO_2 at 220 ^oC and 260 ^oC, respectively, while B and D displays vibration of OCO group on CeO_2 surface at 220 ^oC and 260 ^oC, respectively.

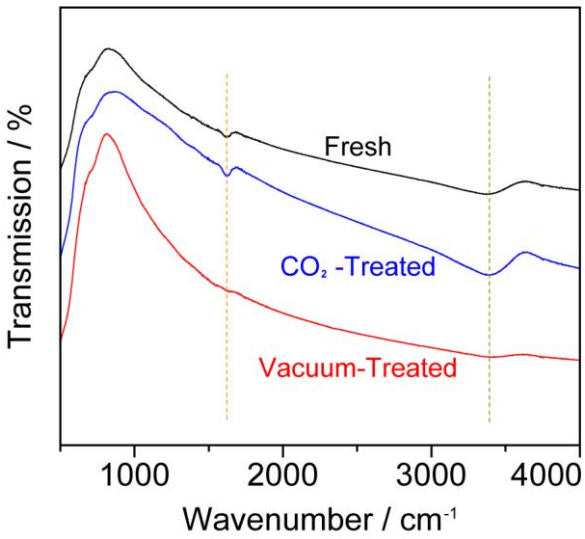

Figure S17. The FT-IR spectra of fresh, CO_2-treated and high-temperature vacuum-treated meso-CeO_2 catalysts.

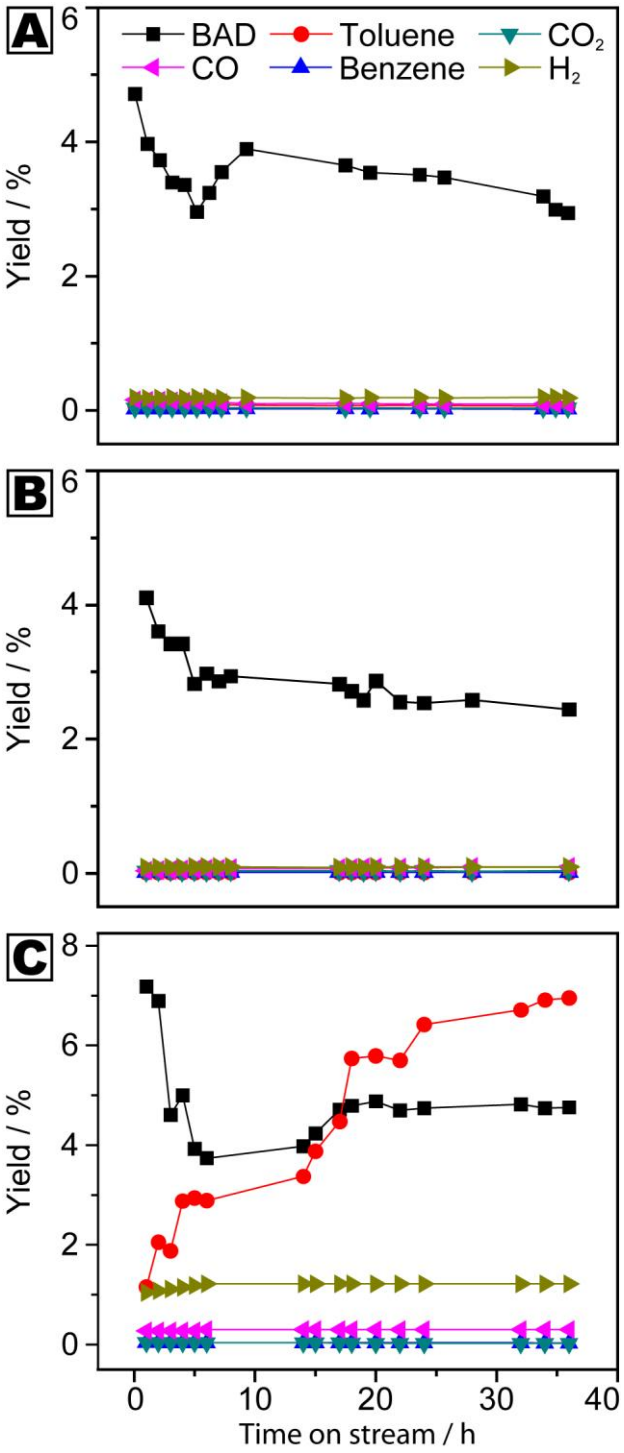

Figure S18. The product yields in anaerobic oxidation of BA over (A) meso-CeO_2 catalyst at 240 ºC; (B) high-temperature vacuum-treated meso-CeO_2 catalyst at 240 ºC; (C) meso-CeO_2 catalyst at 300 ºC. Reaction conditions: catalyst, 0.25 g; BA, 0.4 mL/h; N_2, 20.0 mL/min. The yields of methane were all less than 0.01 % in three processes.

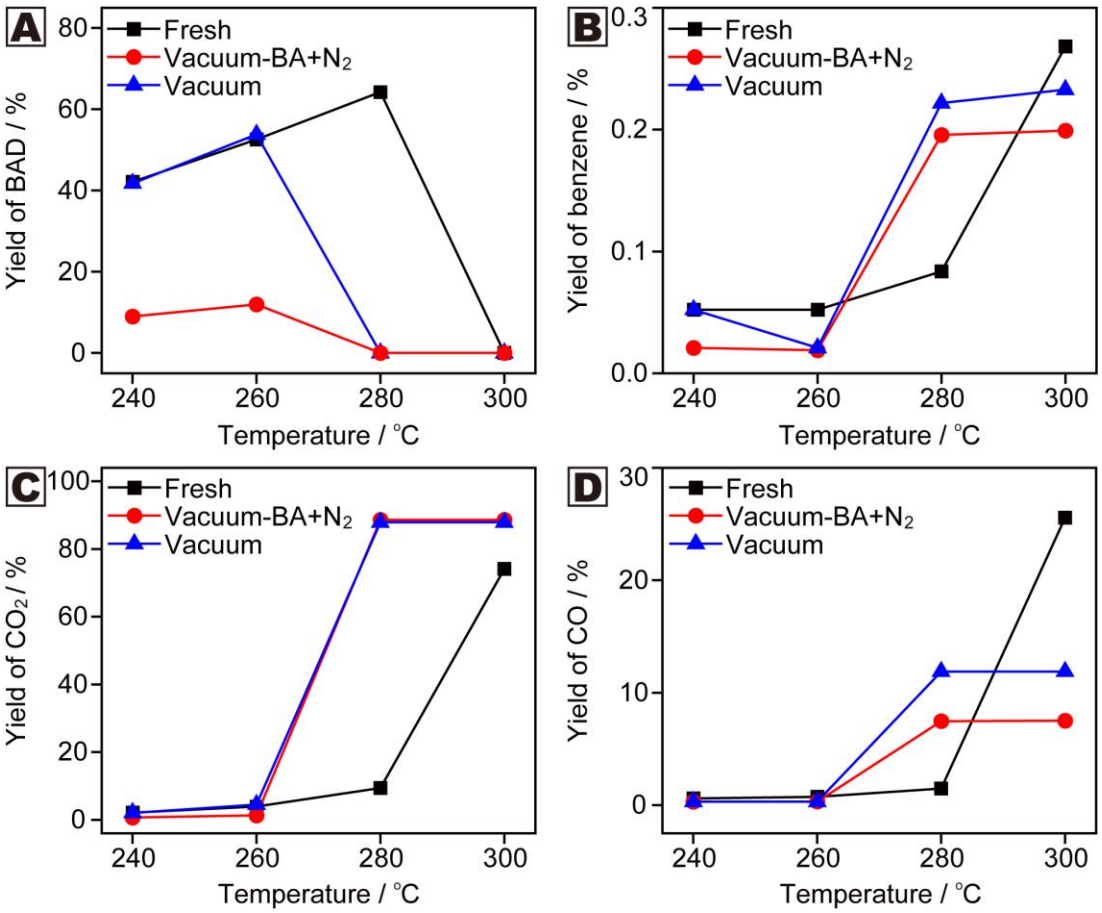

Figure S19. The catalytic performances (the yields of (A) BAD; (B) benzene; (C) CO_2 and (D) CO) in aerobic oxidation of BA over fresh meso-CeO_2 catalyst (Fresh), high-temperature vacuum-treated meso-CeO_2 catalysts before (Vacuum) and after (Vacuum-BA+N_2) aerobic oxidation process of BA at 240 °C for 36 h. Reaction conditions: catalyst, 0.25 g; BA, 0.4 mL/h; O_2, 15.0 mL/min. The yields of methane and toluene were all less than 0.1 % for three catalysts.

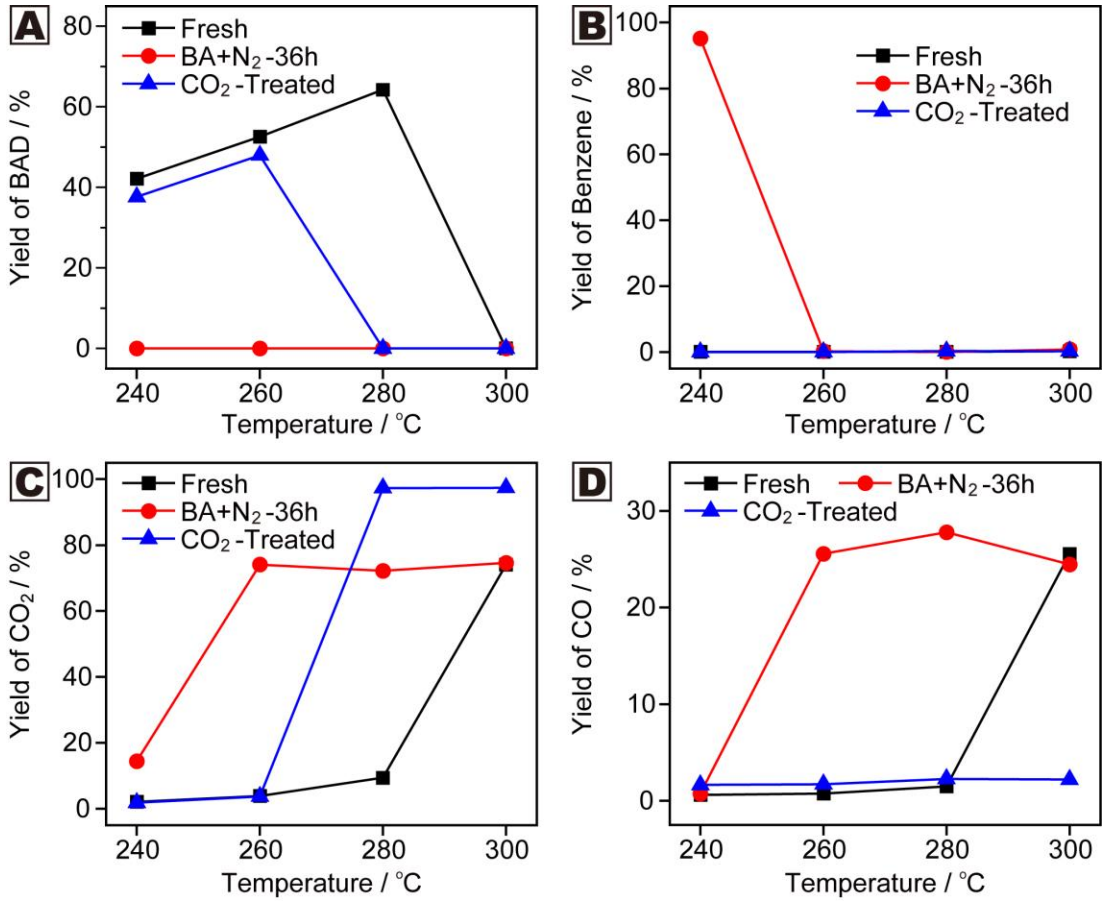

Figure S20. The catalytic performances (Yields of (A) BAD; (B) benzene; (C) CO_2 and (D) CO) in aerobic oxidation of BA over fresh meso-CeO_2 catalyst (Fresh), meso-CeO_2 catalyst after 36 h of CO_2 adsorption at 240 °C (CO_2-treated) and meso-CeO_2 catalyst after 36 h of anaerobic oxidation process at 240 °C (BA-N_2-36h). Reaction conditions: catalyst, 0.25 g; BA, 0.4 mL/h; O_2, 15.0 mL/min. The yields of methane and toluene were all less than 0.1 % for three catalysts.

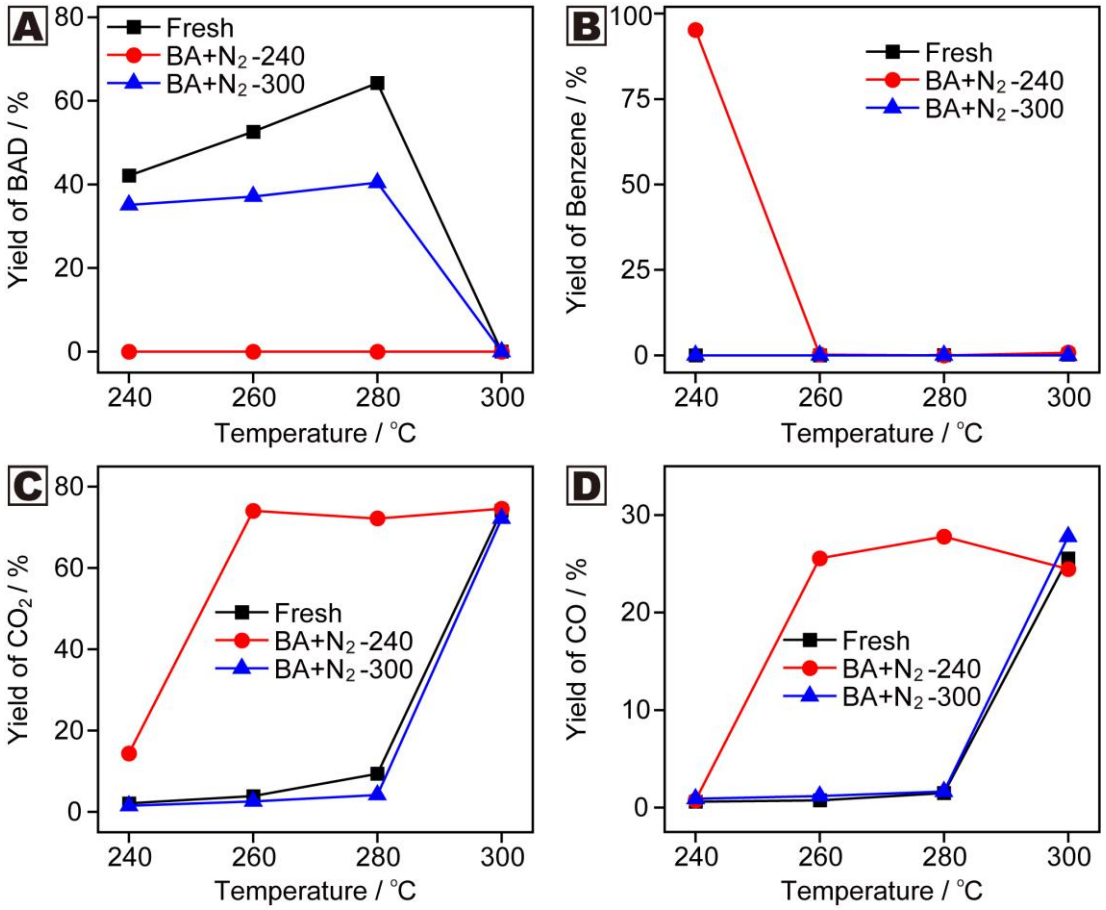

Figure S21. The catalytic performances (the yields of (A) BAD; (B) benzene; (C) CO_2 and (D) CO) in aerobic oxidation of BA over fresh meso-CeO_2 catalyst (Fresh), meso-CeO_2 catalyst after 36 h of anaerobic oxidation process at 240 °C (BA+N_2-240) or 300 °C (BA+N_2-300) respectively. Reaction conditions: catalyst, 0.25 g; BA, 0.4 mL/h; O_2, 15.0 mL/min. The yields of methane and toluene were all less than 0.1 % for three catalysts.

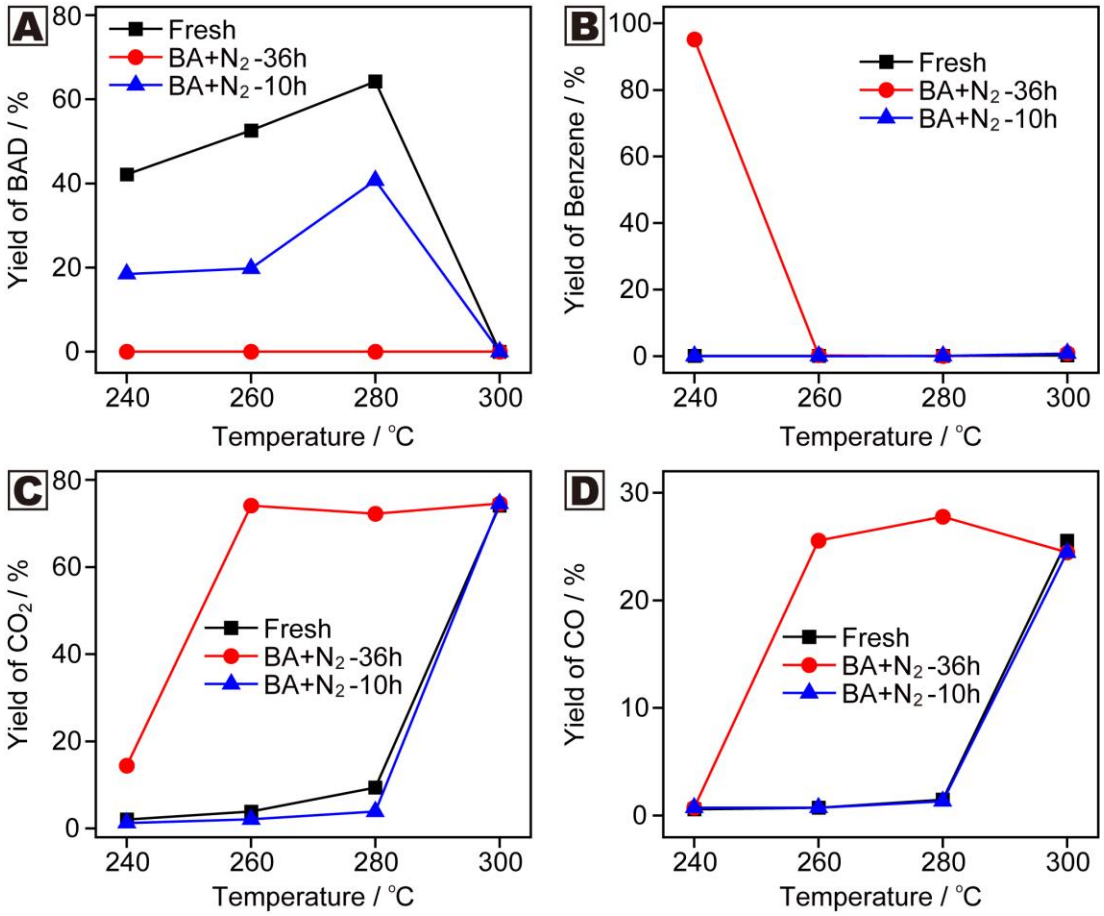

Figure S22. The catalytic performances (the yields of (A) BAD; (B) benzene; (C) CO_2 and (D) CO) in aerobic oxidation of BA over fresh meso-CeO_2 catalyst (Fresh), meso-CeO_2 catalyst after anaerobic oxidation process at 240 °C for 10 h (BA+N_2-10h) or 36 h (BA+N_2-10h), respectively. Reaction conditions: catalyst, 0.25 g; BA, 0.4 mL/h; O_2, 15.0 mL/min. The yields of methane and toluene were all less than 0.1 % for three catalysts.

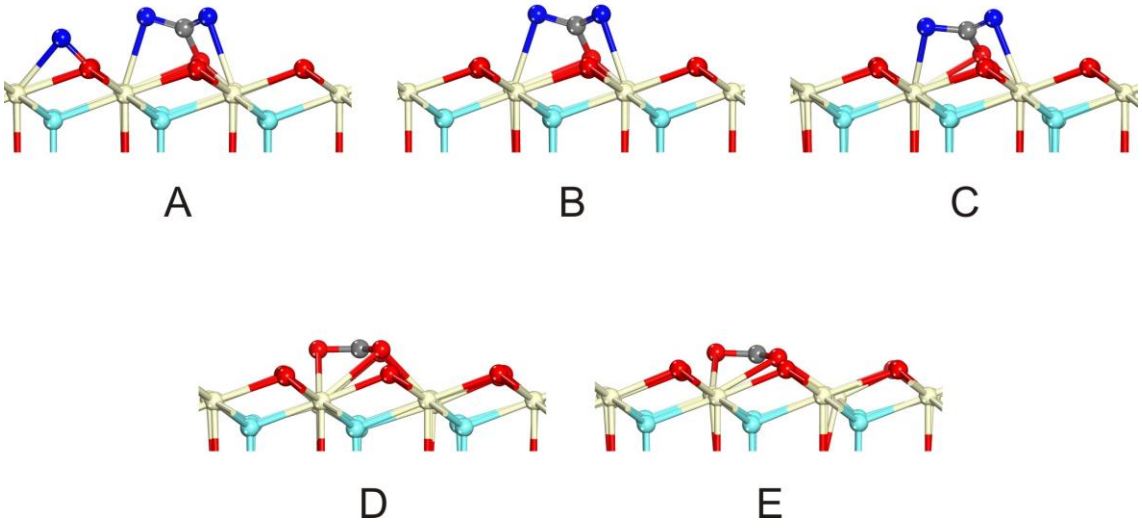

Figure S23. Side views of calculated structures A-E.

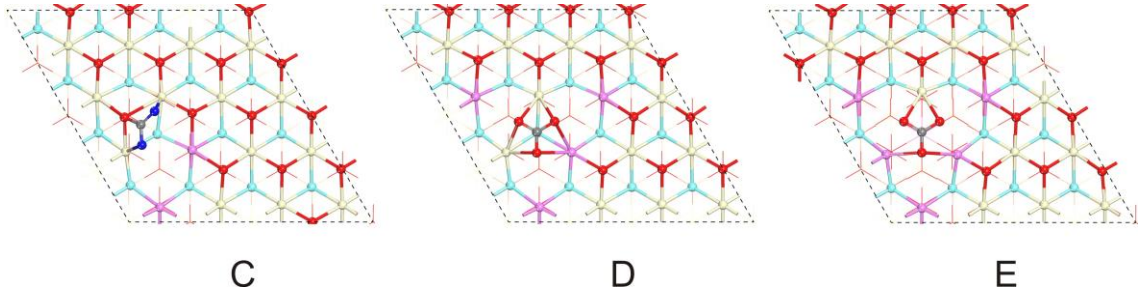

Figure S24. Ce^{3+} distributions of structures C, D and E. Ce^{3+} are pink colored.

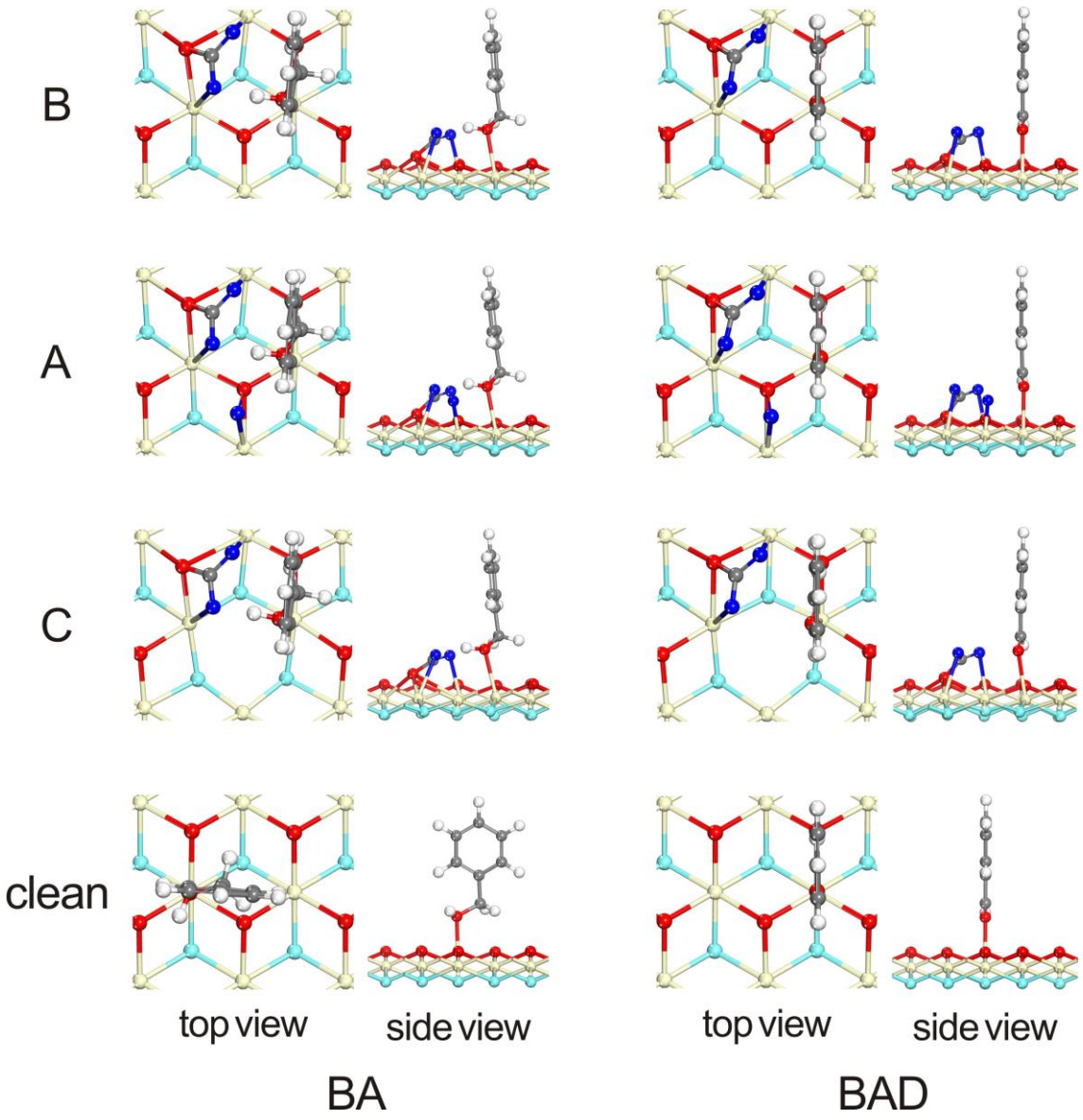

Figure S25. Calculated adsorption structures of BA and BAD at structures B, A, C and clean CeO_2(111). H atoms are in white.

Table S1 Comparison of the catalytic activity of various catalysts (except of Au, Pd, Pt and Ru) in gas-phase selective oxidation of benzyl alcohol.

Catalyst	Reaction Temperature (°C)	Benzaldehyde Selectivity (%)	Specific Activity ($mmol \cdot g_{cat}^{-1} \cdot h^{-1}$)	Reference
3K-Cu-50TiO_2	210	>98	~6	*J. Am. Chem. Soc.* **2009**, *131*, 15568-15569
meso-CeO_2	240	95	26	**This work**
1.0%-V-CeO_2	243	>98	~25	*J. Phys. Chem. C* **2014**, *118*, 24950-24958
Ag/Ni-Microfiber	300	97	179	*Appl. Catal. B. Environ.* **2010**, *99,* 222-228
Ag-HMS-25	310	96	0.7	*Micropor. Mesopor. Mat.* **2012**, *149*, 158-165
1%-Ag/SiO2	320	>99	155	*J. Catal*. **2005**, *234*, 308-317
K-Co/NaUSY	350	99	86	*J. Mol. Catal. A-Chem.* **2006**, *259,* 108-115
Rb-Ce-NaZSM-5	400	79	19	*Phys. Chem. Chem. Phys.,* **1999**, *1*, 373-381
Cu-NaZSM-5	400	84	101	*J. Catal*. **1995**, *153,* 254-264
K-La/NaZSM-5	430	98	59	*J. Mol. Catal. A-Chem.,* **2004**, *211,* 219-226

Table S2.Textural parameters of as-prepared mesoporous CeO_2, commercial 20 nm CeO_2, and commercial bulk CeO_2.

Sample	Crystal size (nm)	Particle size (nm)	Pore size (nm)	Surface area (m^2/g)	Pore volume (cm^3/g)
meso-CeO_2	7.4	8	4.2	56.3	0.084
20nm CeO_2	25.2	30	---	44.3	0.074
bulk CeO_2	---	---	---	7.8	0.023

Table S3. The second highest frequencies ν_{sym}(OCO)) of structures A-E.

A	B	C	D	E
1243 cm^{-1}	1247 cm^{-1}	1240 cm^{-1}	1356 cm^{-1}	1381 cm^{-1}

Table S4. Calculated CO adsorption energies (eV) at structures B, A, C and the clean CeO_2(111) with 1×1×1 and 2×2×1 k-mesh grids.

	Structure B	Structure A	Structure C	Clean surface
1×1×1	1.73	1.53	1.76	0.50
2×2×1	1.73	1.59	1.74	0.48